Majorana chiral spin liquid in a model for Mott insulating cuprates

Jaime Merino
Departamento de Física Teórica de la Materia Condensada, Condensed Matter Physics Center (IFIMAC) and Instituto Nicolás Cabrera, Universidad Autónoma de Madrid, Madrid 28049, Spain

Arnaud Ralko
Institut Néel, Université Grenoble Alpes et CNRS UPR2940, Grenoble 38042, France

(Received 7 January 2022; revised 17 April 2022; accepted 20 April 2022; published 16 May 2022)

The large thermal Hall conductivity recently detected in Mott insulating cuprates has been attributed to chiral neutral spin excitations. A quantum spin liquid (QSL) with Majorana excitations, Chern number ± 4 and large thermal Hall conductivity is found to be an excited state of a frustrated Heisenberg model on the square lattice. Using a Majorana mean-field theory and exact diagonalizations, we explore two possible routes to achieve this chiral QSL, an orbital magnetic-field effect and spin-orbit couplings as present in cuprates. In particular, we show how only the orbital magnetic field allows this topological phase to be the ground state, while it remains an excited state of the Majorana mean field under the Dzyaloshinskii-Moriya terms. A large quantized low-temperature thermal Hall effect can be induced in our model of Mott insulating cuprates by the orbital effect of an applied magnetic field.

DOI: 10.1103/PhysRevResearch.4.023122

I. INTRODUCTION

The pseudogap phase of the cuprates continues to provide unexpected behavior. Thermal Hall experiments have recently found a surprisingly large thermal Hall conductivity [1]. As doping is reduced below the critical doping $\delta < \delta^*$, a negative thermal Hall conductivity signal is observed, which becomes the largest when reaching the Mott insulator $\delta \approx 0$. The large absolute values and T dependence of the thermal Hall conductivity in the undoped cuprate, La_2CuO_4, is very similar to observations in several spin liquid frustrated materials such as volborthite [2] or α-$RuCl_3$ [3]. The half quantization thermal Hall effect [4] observed in α-$RuCl_3$ is interpreted in terms of Majorana edge modes arising in the Kitaev spin liquid under an external magnetic field. It is then an open question whether the Mott and pseudogap phases of cuprates host unconventional neutral chiral excitations which can lead to the observed large thermal Hall effect.

Phonons have been identified as the relevant heat carriers in the thermal Hall effect observed in the pseudogap [5,6] and Mott insulating phases [7] of cuprates. The large values of the thermal Hall conductivity indicates that phonons have nonzero chirality whose origin is yet to be explained. Since magnetic impurity effects and magnons have been discarded, a possible scenario is that the paramagnetic phase of cuprates is a quantum spin liquid (QSL) [8–14] with a nonzero chirality that is imprinted on the phonons through the spin phonon coupling. An intriguing theoretical possibility, which we explore here, is the presence of a chiral QSL with Majorana fermions as elementary excitations similar to the Kitaev QSL relevant to α-$RuCl_3$.

Various chiral QSLs with either bosonic [15] or fermionic spinons [16,17] have been proposed in previous theoretical works of the thermal Hall effect in cuprates. The chiral bosonic spinons [15] and the π-flux phase of fermionic spinons [17] occurring in a Heisenberg model on the square lattice with additional interactions can lead to a large thermal conductivity as observed in cuprates. Similarly, electrons in a d-density wave state [18] induce a large thermal Hall effect as observed in doped Mott insulators. An alternative scenario for an enhanced thermal Hall response in the Mott insulating cuprates is their proximity to a mixed state with coexisting Néel and topological order [16]. Finally, it has been shown how the loop currents proposed in the pseudogap phase induce lattice distortions [6] which can effectively generate a phonon thermal Hall effect consistent with observations.

Here, we show an alternative scenario for the enhanced thermal response in Mott insulating cuprates based on a chiral spin liquid state with Majorana excitations. Using a Majorana representation of the J_1-J_2 Heisenberg model on the square lattice, we find that a chiral spin liquid state breaking time-reversal symmetry with Majorana excitations emerges spontaneously. Such state which we denote as Majorana π-QSL has a large associated Chern number $\nu = \pm 4$, leading to absolute values of the thermal Hall conductivity of the order $\sim k_B^2/\hbar$ as experimentally observed. However, this chiral spin liquid state is only an excited state of the system: the well-known Néel, collinear and/or nonchiral disordered states being favored for different ranges of magnetic frustration.

Extending the Heisenberg model to account for the presence of an external magnetic field through the orbital effect and/or for a Dzyaloshinskii-Moriya (DM) spin-orbit (SO) coupling, we explore whether the π-QSL becomes the absolute (GS) of the system or not. Considering several compatible choices of DM vectors, we show how the π-QSL is lowered in energy by the DM but always remains an excited state of the system. Only the orbital magnetic field is able to turn the π-QSL into the absolute GS, consistent with observations where the magnetic field is essential to externally trigger the transition. Hence the magnetic-field orbital term can drive the model for Mott insulating cuprates into the Majorana π-QSL phase with the large thermal Hall effect as observed experimentally.

II. MODEL AND METHODS

The simplest relevant model to describe the magnetic properties of undoped cuprates is the J_1-J_2 $S = 1/2$ Heisenberg model on the square lattice:

$$H_{\rm H} = J_1 \sum_{\langle ij \rangle} \mathbf{S}_i \cdot \mathbf{S}_j + J_2 \sum_{\langle\langle ij \rangle\rangle} \mathbf{S}_i \cdot \mathbf{S}_j, \tag{1}$$

where the first sum runs over nearest-neighbor sites and the second over next-nearest neighbors.

Electrons can couple to an external magnetic-field B through their orbital motion. A strong coupling expansion of the Hubbard model to $\mathcal{O}(t^3/U^2)$ leads to the additional chiral term [19]:

$$H_\phi = J_\phi \sum_{\triangle} T_{ijk} = J_\phi \sum_{\triangle} \mathbf{S}_i \cdot (\mathbf{S}_j \times \mathbf{S}_k), \tag{2}$$

where $\triangle$ denotes a triangle lying in the square plaquettes of area A with vertices ijk taken in an anticlockwise direction [see Fig. 1(a)]. The three-spin-exchange coupling is $J_\phi = -\frac{24 t_2 t_1^2}{U^2} \sin(2\pi\phi/\phi_0)$, with $\phi = BA/2$ and $\phi_0 = hc/e$ the flux quantum.

A second important ingredient is the SO coupling effect through the DM interaction [20–22] defined as

$$H_{\rm DM} = \sum_{\langle i,j \rangle} \mathbf{D}_{ij} \cdot (\mathbf{S}_i \times \mathbf{S}_j), \tag{3}$$

where $\mathbf{D}_{ij}$ are DM vectors. The compatible vectors $\mathbf{D}_{ij}$ are generically defined by 4 unit vectors $\vec{d}_i$ with $i = 1, 2, 3, 4$ pointing in the different bond directions of a 4-site unit cell, as given in Fig. 1(b). We consider in this work several cases to explore the possibility of SO coupling to lead to a chiral liquid state: SO compatible with cuprates like YBCO, LSCO-LTO, LSCO-LTT as defined in Ref. [15], or SO corresponding to *Rashba-like* and *Dresselhaus-like* couplings [23] (see Appendix D for details).

Finally, we also consider a Zeeman effect term:

$$H_z = -\vec{B} \sum_i \vec{S}_i, \tag{4}$$

in order to explore possible nontrivial competition with the DM SO coupling. Our analysis included in Sec, V shows how adding the Zeeman does not change qualitatively the physics predicted by the DM alone.

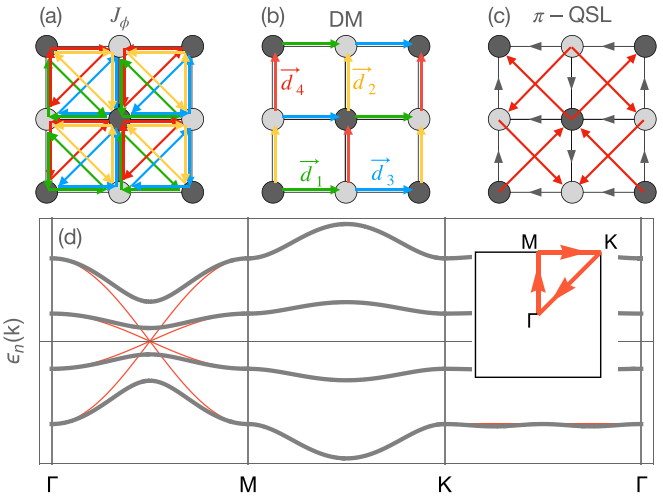

FIG. 1. Majorana chiral QSL state in the J_1-J_2 Heisenberg model on a square lattice. (a) and (b) Bond conventions used for the orbital magnetic-field term and the DM interactions. (c) The bond patterns of the MMFT lowest energy QSL, the π-QSL. The arrows indicate that the bond average phase is $+\pi/2$ ($-\pi/2$) in the same (opposite) direction of the bond. An overall flux of $\pm\pi$ pierces each four-site plaquette. (d) Excitation spectra of the gapless π-QSL for $J_2 = 0$ (red) and of the gapped π-QSL arising for $J_2 \neq 0$ ($J_2 = J_1/2$ in this plot). The Brillouin zone with high-symmetry points is displayed as an inset.

We introduce the Majorana representation of the spins consisting on four Majorana fermion operators c, b^x, b^y, b^z per site as used by Kitaev [24] to exactly solve a highly spin anisotropic model (see Appendix A) on the honeycomb lattice. In this representation, the spin operators are $S_i^\alpha = \frac{i}{2} b_i^\alpha c_i$, where $\alpha = x, y, z$. A three-channel mean-field decoupling of the interaction terms $S_i^\alpha S_j^\beta$ in the Hamiltonian yields to

$$\begin{aligned} &+\tfrac{1}{4}\big[\langle b_i^\alpha i c_i\rangle b_j^\beta i c_j + \langle b_j^\beta i c_j\rangle b_i^\alpha i c_i - \langle b_i^\alpha i c_i\rangle\langle b_j^\beta i c_j\rangle\big] \\ &-\tfrac{1}{4}\big[\langle b_i^\alpha i b_j^\beta\rangle c_i i c_j + \langle c_i i c_j\rangle b_i^\alpha i b_j^\beta - \langle b_i^\alpha i b_j^\beta\rangle\langle c_i i c_j\rangle\big] \\ &+\tfrac{1}{4}\big[\langle b_i^\alpha i c_j\rangle b_j^\beta i c_i + \langle b_j^\beta i c_i\rangle b_i^\alpha i c_j - \langle b_i^\alpha i c_j\rangle\langle b_j^\beta i c_i\rangle\big], \end{aligned} \tag{5}$$

where the first three terms are associated with magnetic orders while the next three with spin liquid formation. With such decoupling, our Majorana mean-field theory (MMFT) [25] allows to analyze on equal footing QSLs($\langle \mathbf{S}_i \rangle = 0$) as well as magnetically ordered states. To do so, as done in Ref. [25], we solve numerically the set of self consistent equations, together with a physical constraint connected to the number of particles per site that our theory has to fulfill.

III. CHIRAL QSL WITH MAJORANA EXCITATIONS

The J_1-J_2 Heisenberg model on the square lattice sustains a chiral QSL state with Majorana fermion excitations (see Appendix A for energy analysis). Among the possible QSL ansätze, the π-flux QSL ansatz or π-QSL from now on, shown Fig. 1(c) has the lowest energy in a finite range of J_2, consistent with Lieb's theorem [27]. The eight corresponding

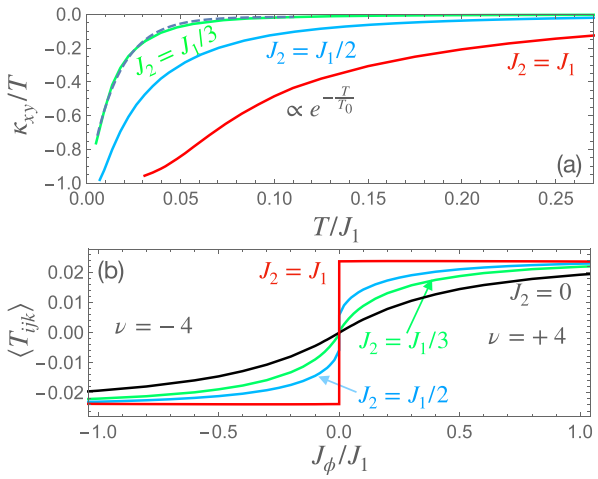

FIG. 2. (a) Thermal Hall conductivity of the π-QSL on the square lattice. The T dependence of κ_{xy}/T in units of $k_B^2/\hbar$ is shown for different J_2/J_1. The π-QSL leads to large absolute values of $\kappa_{xy}/T \sim -k_B^2/\hbar$ as $T \to 0$ and an intermediate T dependence [26], $\kappa_{xy}/T \propto e^{-\frac{T}{T_0}}$, consistent with observations in undoped cuprates. From such exponential fit to the $J_2 = J_1/3$ theoretical results we obtain a $T_0 \approx 18$ K (assuming $J_1 \sim 0.1$ eV), very close to experimental values, $T_0^{expt} \approx 16-18$ K for La_2CuO_4 and $Sr_2CuO_2Cl_2$. (b) Dependence of the chirality of the π-QSL state with J_ϕ obtained from MMFT. Dependence of the Chern number of the π-QSL state with J_ϕ for all J_2.

Majorana bands – there are two sites per unit cell [28], labeled A and B – are given by $\pm 3\gamma(\mathbf{k})$, $\pm\gamma(\mathbf{k})$ (triply degenerate) with

$$\gamma(\mathbf{k}) = \frac{J_1}{2}\sqrt{c_1^2(\sin^2 k_x + \cos^2 k_y) + \left(2\frac{J_2}{J_1}c_2 \cos k_x \sin k_y\right)^2},$$

where we have defined $c_1 = \langle c_{i_A} i c_{j_B}\rangle = \langle b^\alpha_{i_A} i b^\alpha_{j_B}\rangle$ and $c_2 = \langle c_{i_A} i c_{j_A}\rangle = \langle b^\alpha_{i_A} i b^\alpha_{j_A}\rangle$. For $J_2 = 0$, all these bands touch at the two Dirac points $(0, \pm\pi/2)$ in the Brillouin zone as shown in Fig. 1(d), the π-QSL is gapless in this case. Moreover, it minimizes the total energy with $E = -0.3442J_1$ which is lower than the 0-flux QSL energy. The $\pm\pi$ Berry phases at the Dirac cones can lead to nontrivial topology if the gap opens in a nontrivial manner. Indeed, this occurs when turning on a $J_2 \neq 0$, as shown in Fig. 1(d). The gap opening lowers slightly the energy from $E = -0.3442J_1$ ($|c_1| = 0.4790$) for $J_2 = 0$ to $E = -0.3443J_1$ ($|c_1| = 0.4777$, $|c_2| = 0.0516$) for $J_2 = 0.5$ and to $E = -0.3726J_1$ ($|c_1| = 0.4189$, $|c_2| = 0.2700$) for $J_2 = J_1$. Moreover, a direct calculation of the topological invariant Chern number ν on the occupied Majorana bands [25] (with negative energy) shows that this state is a gapped topological π-QSL with $\nu = \pm 4$.

In Fig. 2(a) we show the thermal Hall conductivity of the π-QSL obtained from the expression [29]

$$\frac{\kappa_{xy}}{T} = \frac{k_B^2}{\hbar}\frac{1}{8(k_B T)^3}\int d\epsilon \frac{(\epsilon-\mu)^2}{\cosh^2[\beta(\epsilon-\mu)/2]}\sigma_{xy}(\epsilon), \quad (6)$$

where $\sigma_{xy}(\epsilon) = -\sum_{n\mathbf{k}} \Omega_n^z(\mathbf{k})\theta(\epsilon - \epsilon_n(\mathbf{k}))$. Note that the r.h.s. of Eq. (6) is half of the standard expression used for fermionic spinons since in our MMFT approach, thermal energy is transported by the Majoranas. In the limit $T \to 0$, we have $\kappa_{xy}/T = -\frac{\pi k_B^2}{12\hbar}\sum_{n\in\text{filled}} \nu_n \to -2(\frac{\pi k_B^2}{6\hbar})$ since each of the four occupied bands carries a Chern number $\nu_n = +1$. Hence the thermal Hall effect is integer quantized in units of $(\frac{\pi k_B^2}{6\hbar})$ which is strong evidence of a chiral QSL. In comparison, the thermal Hall effect of the Kitaev Z_2 spin liquid under weak magnetic fields is $\frac{1}{2}(\frac{\pi k_B^2}{6\hbar})$, i.e., it is half quantized since there is a single Majorana edge mode carrying heat. Although the overall absolute values of κ_{xy}/T are consistent with observations (see Appendix B for a detailed comparison) there is no experimental evidence for the integer quantization of κ_{xy}/T at least down to the lowest temperatures of $T \sim 8$ K reached. As temperature is raised and thermal excitations of the Majorana fermions occur, there is a cancellation between Chern numbers of the bands above and below zero energy and $\kappa_{xy}/T \to 0$. Overall the T dependence predicted is consistent with experimental observations in the undoped cuprate La_2CuO_4. Although the magnitude of κ_{xy}/T is also consistent with experiments, there is no evidence for the quantization of κ_{xy}/T predicted here.

The gapped π-QSL found in the J_1-J_2 Heisenberg model for $J_2 \neq 0$ is doubly degenerate since there are two possible senses of the bond amplitudes or chiralities, $\langle T_{ijk}\rangle \neq 0$, with the same energy. Hence the Chern number of the π-QSL can have two values, $\nu = \pm 4$, depending on the sign of the chirality as shown in Fig. 2(b). It may seem that spontaneous symmetry breaking can occur since any infinitesimal $J_\phi \to 0^\pm$ selects either the $\nu = 4$ or the $\nu = -4$ π-QSL solution. However, our MMFT stability analysis below reveals that the π-QSL is only an excitation of the pure $J_1 - J_2$ Heisenberg model. Under a finite J_ϕ, the π-QSL with the favorable sign of the chirality for the orientation of the applied B, becomes the GS of the system. This is consistent with experiments on the cuprates which find no thermal Hall effect when no magnetic field is applied implying no spontaneous time-reversal symmetry-breaking GS.

IV. ORBITAL MAGNETIC FIELD EFFECT

We have performed fully self-consistent MMFT calculations on the J_1-J_2-J_ϕ model. The Majorana mean-field decoupling of the three-spin term is described in detail in Appendix C. The resulting phase diagram shown in Fig. 3 displays Néel, stripe, and spin disordered phases. For $J_\phi = 0$ we qualitatively recover the phase diagram of the J_1-J_2 Heisenberg model on the square lattice. Subject of an intense research activity since the discovery of cuprate superconductivity, recent state-of-the-art numerical works [30–33] find a gapless QSL and a valence bond solid around $J_2/J_1 \sim 0.5$. Our MMFT is partially consistent with this since it predicts a spin disordered valence bond crystal (VBC) phase sandwiched between the magnetically ordered Néel and collinear phases. Note that, at the mean field level, all VBCs like the columnar or the staggered phases, as well as possible resonating plaquette phases [28] are degenerate all consisting of disconnected singlets. On the other hand, under sufficient strong J_ϕ, the MMFT finds that the π-QSL becomes the

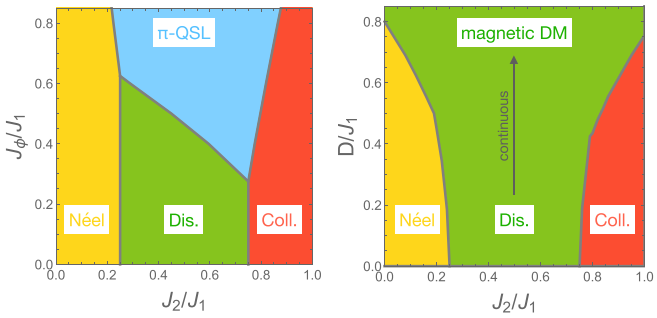

FIG. 3. Phase diagrams of the J_ϕ and D models obtained from MMFT for cluster of $2 \times 32 \times 32$ sites. Left: Orbital magnetic field, J_ϕ, model. The intermediate phase (blue region) is the π-flux QSL with topological Chern number of $\nu = \pm 4$. Right: DM, D model. For any choice of the DM couplings, a spin disordered phase is stabilized and a continuous transition to the respective classical magnetic state is observed (arrow).

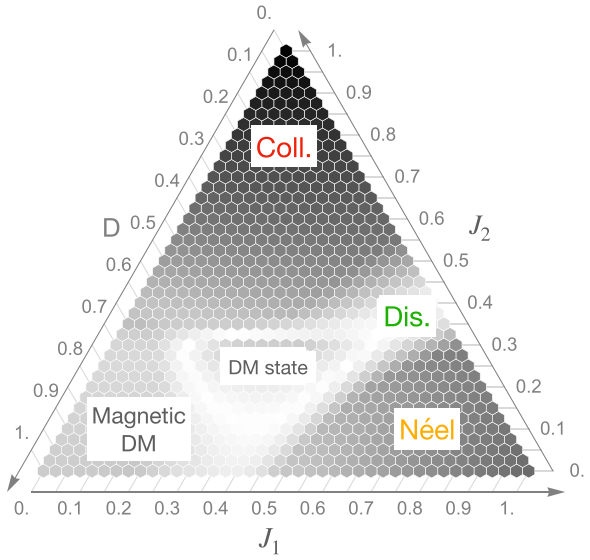

FIG. 4. Density map of the gap ΔE on a ternary plot satisfying $J_1 + J_2 + D = 1$ obtained by ED on the 16-site cluster. The more white the density, the smaller the gap. Five phases are observed: The Néel, the disordered and the collinear phases from the original $J_1 - J_2$ model that largely extend in the phase diagram, an ordered phase driven by D called magnetic DM, and a trivial and possibly disordered intermediate phase dubbed the DM state, delimited by frontiers of zero gap (white lines).

GS in a broad region of the J_2-J_ϕ phase diagram. Although nonphysical large J_ϕ values are needed, it is well known that mean-field theory overestimates broken symmetry states. Indeed, we show below how quantum fluctuation effects strongly suppress the critical J_ϕ at which the π-QSL emerges in the phase diagram.

V. SO COUPLING EFFECT

We now analyze the effect of the DM interaction parameterized by the **D** vectors. In this section, we discuss the phase diagram of the J_1-J_2-D model in the presence of a SO coupling that forces the spin rotations to be coupled with real-space symmetry transformations. The DM term is defined as

$$H_{\rm DM} = \sum_{\langle i,j \rangle} \vec{D}_{ij} \cdot (\vec{S}_i \times \vec{S}_j), \tag{7}$$

where $\vec{D}_{ij}$ are the DM vectors. We consider three DM vector choices compatible with YBCO, LSCO-LTO, LSCO-LTT cuprates, and two DM vector choices realizing Rashba-like and Dresselhaus-like SO as observed in the electronic systems considered by [23]. The corresponding $\vec{d}_i$ vectors as displayed in Fig. 1 are defined as (i) YBCO with $\vec{d}_1 = \vec{d}_3 = (d, 0, 0)$ and $\vec{d}_2 = \vec{d}_4 = (0, -d, 0)$, (ii) LSCO-LTO with $\vec{d}_1 = -\vec{d}_3 = (d, 0, 0)$ and $\vec{d}_2 = -\vec{d}_4 = (0, -d, 0)$, (iii) LSCO-LTT with $\vec{d}_1 = -\vec{d}_3 = (0, d, 0)$ and $\vec{d}_2 = -\vec{d}_4 = (0, d, 0)$, (iv) *Rashba* with $\vec{d}_1 = \vec{d}_3 = (0, d, 0)$ and $\vec{d}_2 = \vec{d}_4 = (-d, 0, 0)$ and (v) *Dresselhaus* with $\vec{d}_1 = \vec{d}_3 = (0, -d, 0)$ and $\vec{d}_2 = \vec{d}_4 = (-d, 0, 0)$. The effect of the DM term can be considered by employing the MMFT as described in Appendix D. Three important features can be inferred from the phase diagram of Fig. 3. First, the π-QSL is always a stable ansatz of our MMFT. Second, the VBC is always lower in energy than the π-QSL, whatever the choice of the DM vectors. Finally, the π-QSL is also always lowered with respect to D indicating that the effect of SO coupling is positive, in the sense that it continues to favor it even though it is an excited state (see Appendix D).

To further understand the role of the DM term, we have solved the $J_1 - J_2 - D$ Hamiltonian by using exact diagonalizations (EDs) on a 16 site cluster and the MMFT for the case compatible with YBCO compounds. In Fig. 4, we show a ternary plot with the constraint $J_1 + J_2 + D = 1$, of the first gap obtained by ED. We immediately see five distinct domains separated by zero gap lines (white regions). Along the $D = 0$ line, we recover the Néel region (close to $J_1 = 1$), the intermediate disordered phase ($0.4 < J_2 < 0.6$) and the collinear phase at higher J_2. We have characterized these phases by calculating the quantum fidelity $|\langle \psi_{\rm ref} | \psi_0 \rangle|$ in the whole parameter space by starting from four reference states $|\psi_{\rm ref}\rangle$ chosen deep in their corresponding expected parameter regions (see Appendix D).

To conclude this section, we want to briefly discuss the role of the Zeeman term in our model. While it is known that the combination of SO coupling and the presence of an external magnetic field can induce a scalar spin chirality, it is not the case here. We have added the Zeeman term $H_z = -\vec{B} \sum_i \vec{S}_i$ in the Hamiltonian and have checked for both ED and MMFT the effect of the magnetic field for the different DM vectors considered. As an example, we show in Fig. 5 the energy gap obtained by ED along lines of the ternary phase diagram, $J_1 = J_2$ and $J_2 = D$ with the constraint $J_1 + J_2 + D = 1$ and for various $\vec{B} = B\vec{u}_z$. As it can been seen, the physical picture remains unchanged for the $J_2 = D$ scan, and only the phase boundaries are slightly shifted with respect to $\vec{B}$ and eventually the magnetic orders are destroyed by magnetic polarization when B is strong enough e.g. on the gray curve at $B = 0.8$. For $J_1 = J_2$ though, a stronger effect is observed at $B = 0.4$ where a gap closing appears in the disordered region. Our numerical analysis cannot find clear signatures of topological order so we conclude that this phase is trivial.

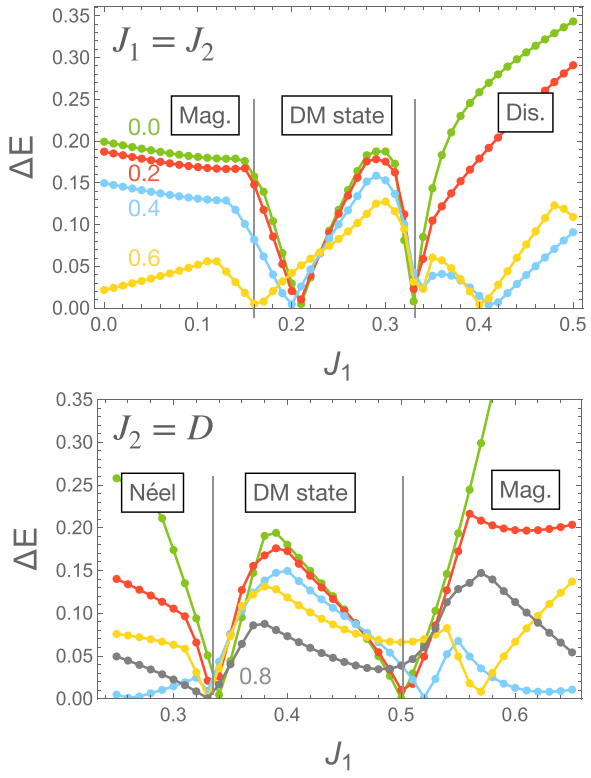

FIG. 5. Role of the Zeeman term $H_z = -\vec{B}\sum_i \vec{S}_i$ on the system with DM interaction (YBCO in this case) for two scans with the constraint $J_1 + J_2 + D = 1$: $J_1 = J_2$ (up panel) and $J_2 = D$ (down panel). The strength of the magnetic-field B is 0.0 (green), 0.2 (red), 0.4 (blue), 0.6 yellow, and 0.8 (gray).

VI. RELATION OF MMFT WITH FERMIONIC SPINON MEAN-FIELD THEORIES

The MMFT we have used leads to the exact solution of the highly anisotropic Kitaev model [24]. Then the question arises: Does it make any sense to apply the MMFT to very different models such as the isotropic frustrated Heisenberg model on a square lattice (with additional interactions) explored here? The answer to this question is given, in part, by Kitaev [24], who noted that mean-field states with the decouplings of the type of Eq. (5) could actually occur in frustrated Heisenberg antiferromagnets (AFs) and have energies lower than competing magnetically ordered states. Our work goes in this direction and finds that indeed the Majorana π-QSL state is the GS of the $J_1 - J_2 - J_\phi$ model in certain parameter range. This means that competing interactions on the spins, even on a square lattice, can allow for Majorana collective modes.

So let us compare our MMFT results with previous alternative mean-field theories [16,17] in which the spin operator is decoupled in terms of Abrikosov fermions instead: $\mathbf{S}_i = \frac{1}{2} f^\dagger_{i\alpha} \sigma^\alpha f_{i\alpha}$. In contrast to our MMFT π-QSL, the spinon π-flux state introduced in Ref. [17] leads to a zero thermal Hall effect on the half filled square lattice in the $T \to 0$ limit. This is due to a cancellation of the spin-up and spin-down counterpropagating spinon edge states. As we have shown, our π-QSL state has a large thermal Hall effect. On the other hand the spinon mean-field approach of Ref. [16], which considers the orbital magnetic-field effect, leads to a chiral spin liquid in which spin-up and spin-down spinon edge states circulate in the same direction leading to a large thermal Hall effect with the same absolute values as found in our Majorana π-QSL: $|\kappa_{xy}/T| = \frac{\pi}{3}\frac{k_B^2}{\hbar}$. In essence our eight Majorana bands correspond to the four spinon bands of Ref. [16]. Since each spinon band has $\nu_n = \pm 1$ and only two are occupied at half filling $|\kappa_{xy}/T| = \frac{\pi k_B^2}{6\hbar}\sum_{n\in\text{filled}} \nu_n = \frac{\pi}{3}\frac{k_B^2}{\hbar}$ as we find with the MMFT. Hence the large thermal Hall effect observed can be equally described in terms of fermionic spinon or Majorana excitations. Although the two approaches may seem equivalent regarding the thermal Hall effect, they lead to different types of physical excitations. This suggests that other experimental probes apart from thermal Hall experiments are needed to search for Majoranas in Mott insulating cuprates and to be able to distinguish them from spinon excitations. It is worth adding that, despite many years of intense research, there is no conclusive evidence of the existence of spinons in two-dimensional (2D)quantum magnets. Hence it remains an experimental challenge how to unambiguously determine the nature of the elementary quasiparticles in these systems.

Additionally we note that, typically, such mean-field Abrikosov fermion theories do not fully solve the associated self-consistent equations and compare the energy of the π-flux chiral spin liquid ansatz with other competing states. Hence it is unclear if the spinon version of the π-flux chiral spin liquid is the actual GS of the system. In contrast, our full energy analysis does show how the Majorana π-QSL is indeed the lowest energy state of the $J_1 - J_2 - J_\phi$ Heisenberg model in certain parameter range.

VII. BEYOND MMFT

We now explore quantum fluctuation effects not contained in the MMFT using ED techniques. There has been intense research activity around the Heisenberg model on the square lattice. The bare $J_1 - J_2$ Heisenberg model on the square lattice displays a spin disordered region between the magnetically ordered Néel and collinear state around [34,35] $J_2/J_1 \sim 0.5$. The character of such intermediate disordered state remains controversial with the most recent work [30–33] finding a QSL for $0.4 \leqslant J_2/J_1 < 0.5$ and a VBC for $0.5 < J_2/J_1 < 0.6$. Several studies have found a chiral QSL of the Kalmeyer-Laughlin [36] type [37,38] in $J_1 - J_2$ Heisenberg model. In contrast, under the combined effect of a DM and a Zeeman term, an AF state with nonzero Berry curvature occurs [15,39].

An important question is whether the π-QSL can occur beyond the MMFT approach. In Fig. 6 we show the quantum fidelity $|\langle\psi_{\text{ref}}|\psi_0\rangle|$ where $|\psi_0\rangle$ is the GS for a given set of parameters and $|\psi_{\text{ref}}\rangle$ is a reference state at known limiting values of the parameters (see caption of Fig. 6 and Appendix F for more details). For $J_\phi = D = 0$, we identify the Néel and collinear phases a well as a possible disordered phase around $J_2 \sim 0.5 - 0.7$. We also find that the phases shown in Fig. 6 arising between the Néel and collinear phase under J_ϕ or under D are quite different. ED calculations of the spin structure factor (see Appendix E) and spin chirality $\langle T_{ijk}\rangle$ suggest that,

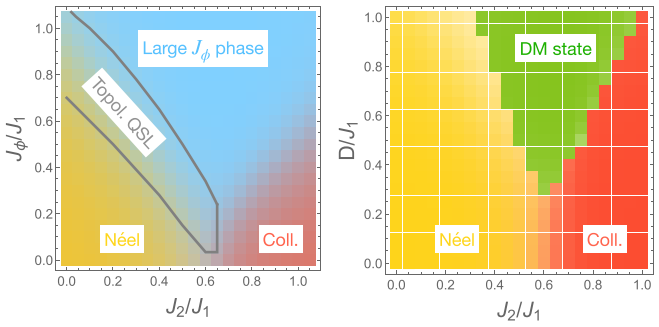

FIG. 6. Phase diagrams of the J_ϕ and D models (illustrated for YBCO) obtained from ED calculations on a 4×4 cluster based on a quantum fidelity analysis. The more intense the color, the closest to 1 the fidelity. Three reference states are used: (i) The pure Néel at point $J_2 = J_\phi = D = 0$ (yellow); (ii) the collinear state $J_2 = 1, J_\phi = D = 0$ (red); and (iii) the intermediate phases at $J_2 = 0.65, J_\phi = 1.0, D = 0$ (blue), and $J_2 = 0.6, J_\phi = 0, D = 1$ (green). Left: Orbital magnetic field, J_ϕ model presenting an intermediate topological QSL. Right: DM, D model and its first-order transition to a DM state driven by D.

while the intermediate phase is spin disordered (blue region) and chiral, $\langle T_{ijk} \rangle \neq 0$, in the J_ϕ model, in the D-model it is nonchiral, $\langle T_{ijk} \rangle = 0$ and possibly also spin disordered as discussed below (green region). It however has to connect with the pure D limit at which magnetic order induced by D eventually sets in. Based on the consistent comparison of the ED phase diagram of Fig. 6 and the MMFT phase diagram of Fig. 3, we associate the (blue) spin disordered phase region with the MMFT π-QSL and the (green) magnetic DM with MMFT DM magnetically ordered phase.

Within the intermediate spin disordered phase of the J_ϕ model, close to the Néel phase, we find a topological QSL. This QSL is chiral [40,41] characterized by a nonzero Chern number, $\nu = 1$, associated with a two-fold degenerate GS well separated from a continuum of excited states, as reported previously [37]. Interestingly this phase survives down to very low J_ϕ for $J_2 \sim 0.6$ as shown in Fig. 6. In the D-model, the evidence for a distinct and possibly spin disordered phase is corroborated by calculations combining the quantum fidelity, the gap and the spin structure factor. Indeed, in contrast to the orbital magnetic-field case, the spin phase induced by D is clearly delimited by a gap closing associated with level crossings (see Appendix D) suggesting, to the best of our knowledge, a novel intermediate phase induced by SO coupling. We let the analysis of this phase as a future work.

Chiral QSLs have been found to be exact GSs of $S = 1/2$ spin models containing the orbital effect of the magnetic field, H_ϕ, on the square [37,40,41] and the triangular lattice [42]. A non-Abelian QSL can also be stabilized by H_ϕ in a $S = 1$ spin model on the triangular lattice [43,44]. Also a chiral QSL has been found in the triangular lattice with four-spin terms [45] as well as in spin models of Kagomé Mott insulators [46–49]. Thus the MMFT could help determining the nature of these chiral QSLs.

VIII. CONNECTION WITH CUPRATE MATERIALS

In cuprates [50] $t_1 \sim 0.45$ eV, $U \sim 8$ eV, $J_1 \sim 0.1$ eV, and $t_2 \sim 0.35 t_1$ (YBCO), $t_2 \sim 0.15 t_1$ (LSCO) so that $J_2/J_1 \sim 0.12$ (YBCO), and $J_2/J_1 \sim 0.023$ (LSCO). Since DM is only of a few meV, $D/J \lesssim 0.1$, we would predict that the system under no magnetic field is in the Néel phase as indeed is observed in undoped cuprates. If a magnetic field of $B \sim 10$ T is applied to the system, the flux term, $J_\phi/J_1 \sim 10^{-4} - 10^{-3}$ would be tiny. Based on the phase diagrams obtained here, in such parameter range appropriate for cuprate materials, $J_2/J_1 \sim 0.1$ and $J_\phi \to 0$, the system would be immersed in the Néel phase and so no thermal Hall effect would be expected based on our analysis. However, since the MMFT finds (see Appendix A) that the π-QSL can coexist with the Néel AF, the π-QSL amplitude in the GS can still lead to a large thermal Hall effect under J_ϕ. Such hybrid π-QSL + Néel AF state may also account for the anomaly observed around $(\pi, 0)$ in the magnon dispersion of square lattice AFs [51] which could result from the decay of $S = 1$ magnons into a continuum of Majorana excitations associated with the π-QSL.

We note that a more complete model for the cuprates would include the four-spin terms arising at $O(t^4/U^3)$ in a large U/t expansion of the Hubbard model [52]. For instance, in the triangular lattice [19,45] these terms stabilize a gapless QSL with an spinon Fermi surface. Since such term is t/U smaller than the three-spin term, we believe that our π-QSL chiral state remains stable under this additional perturbation. However, including these higher-order terms in our MMFT is beyond the scope of the present work and so this question remains open.

IX. CONCLUSIONS

We report a novel chiral QSL state with Majorana excitations and Chern number $\nu = \pm 4$ which occurs as an excited state of the Heisenberg model on the square lattice. MMFT predicts that this Majorana π-QSL becomes the GS under sufficiently large J_ϕ consistent with a topological chiral QSL found in ED. The thermal Hall conductivity of this Majorana π-QSL is quantized with large absolute values $|\kappa_{xy}/T| \sim (k_B^2/\hbar)$ as $T \to 0$. Our analysis then indicates that a large low-temperature thermal Hall effect consistent with observations in Mott insulating cuprates can be induced in the $J_1 - J_2$ Heisenberg model by the orbital effect of an applied magnetic field. The DM present in cuprates plays a secondary role, eventually lowering critical J_ϕ's toward more physically realistic values, so does the combination of the Zeeman term with DM, which is shown to only change the boundaries of the phase diagrams without providing nontrivial features.

ACKNOWLEDGMENTS

J.M. acknowledges financial support from (RTI2018-098452-B-I00) MINECO/FEDER, Unión Europea and the María de Maeztu Program for Units of Excellence in R&D (Grant No. CEX2018- 000805-M).

APPENDIX A: MMFT OF THE HEISENBERG MODEL ON A SQUARE LATTICE

We first provide the details of the MMFT performed on the $J_1 - J_2$ Heisenberg model on a square lattice. We introduce the Majorana representation of the spin operators [24]

$$S_i^\alpha = \frac{i}{2} b_i^\alpha c_i, \tag{A1}$$

where $\alpha = x, y, z$.

It is worth comparing the MMFT with the more widely used Abrikosov fermion theories as previously noted [53]. This expression can be derived by expressing the Abrikosov fermion representation of the spin operator in terms of Majorana fermions

$$S_i^\alpha = \tfrac{1}{2} f_{i\sigma}^\dagger \tau_{\sigma\sigma'}^\alpha f_{i\sigma'} = \tfrac{1}{4}\left(i b_i^\alpha c_i - i b_i^\beta b_i^\gamma\right), \tag{A2}$$

where α, β, γ are cyclic indices for x, y, z,so, for example, $S_i^x = \frac{1}{4}(i b_i^x c_i - i b_i^y b_i^z)$. The single occupancy constraint of the Abrikosov fermions $\sum_\alpha f_{i\alpha}^\dagger f_{i\alpha} = 1$ is equivalent to $b_i^x b_i^y b_i^z c_i = 1$ which implies that $i b_i^\alpha c_i = -i b_i^\beta b_i^\gamma$. Substituting the constraints in the Eq. (A2) we recover the spin operators (A1). Hence by introducing the spin operators $S_i^\alpha = \frac{i}{2} b_i^\alpha c_i$ in the Hamiltonian the constraint is automatically taken into account. It can be shown how a mean-field decoupling of the Kitaev model written in terms of (A1) recovers the exact GS energy. This is in contrast with a conventional mean-field Abrikosov fermion decoupling of the Kitaev model in which the single occupancy constraint would only be treated on average $\sum_\alpha \langle f_{i\alpha}^\dagger f_{i\alpha}\rangle = 1$ leading to a ground-state energy which is a factor of four smaller than the exact energy of the Kitaev model [53] leading to the wrong conclusion that a magnetically ordered state wins over the Kitaev QSL.

Hence our approach performs a mean-field decoupling of the Heisenberg interaction terms expressed using Eq. (A1) and additionally imposes the set of constraints,

$$\begin{aligned} b_i^z c_i &= b_i^y b_i^x, \\ b_i^y c_i &= b_i^x b_i^z, \\ b_i^x c_i &= b_i^z b_i^y, \end{aligned} \tag{A3}$$

on average by introducing three Lagrange multipliers, λ_i, $i = x, y, z$. Including these constraints in the MMFT has proved essential [25] to naturally account for the opening of a topological gap in the Kitaev model under a uniform magnetic field as first found by Kitaev [24]. As discussed above, this is not equivalent to a mean-field decoupling using an Abrikosov fermion representation since the single occupancy constraint would be incorporated only on average. In particular, QSL states in the Abrikosov fermion picture would be unfavored with respect to magnetically ordered phases [53].

Any bilinear of spins $S_i^\alpha S_j^\beta$ can be mean-field Hartree-Fock decoupled as

$$\begin{aligned} &+\tfrac{1}{4}\left[\langle b_i^\alpha i c_i\rangle b_j^\beta i c_j + \langle b_j^\beta i c_j\rangle b_i^\alpha i c_i - \langle b_i^\alpha i c_i\rangle\langle b_j^\beta i c_j\rangle\right] \\ &-\tfrac{1}{4}\left[\langle b_i^\alpha i b_j^\beta\rangle c_i i c_j + \langle c_i i c_j\rangle b_i^\alpha i b_j^\beta - \langle b_i^\alpha i b_j^\beta\rangle\langle c_i i c_j\rangle\right] \\ &+\tfrac{1}{4}\left[\langle b_i^\alpha i c_j\rangle b_j^\beta i c_i + \langle b_j^\beta i c_i\rangle b_i^\alpha i c_j - \langle b_i^\alpha i c_j\rangle\langle b_j^\beta i c_i\rangle\right], \end{aligned} \tag{A4}$$

where the first three terms are associated with magnetic ordering while the rest with spin liquid formation. This decoupling is performed on the Heisenberg terms of the Hamiltonian ($\alpha = \beta$). The constraints in Eq. (A3) are enforced at the mean-field level through the set of Lagrange multipliers, $\{\lambda_i\}$. Since there is no contribution from the last three terms we neglect them in our present analysis.

In order to be able to describe collinear phases, four-site unit cells are used in actual calculations. Here we describe the implementation of the MMFT equations assuming a two-site unit cell allowing for Néel and/or π-flux QSL states. The diagonalization of the Hamiltonian is performed in momentum space by first performing a Fourier transform of the Majoranas,

$$c_j^a = \sqrt{\frac{2}{N_c}} \sum_{\mathbf{k}} e^{i\mathbf{k}\mathbf{R}_j} c^a(\mathbf{k}), \tag{A5}$$

where we have used here, for convenience, the notation $c_j^0 = c_j$, $c_j^1 = b_j^x$, $c_j^2 = b_j^y$, $c_j^3 = b_j^z$. On the other hand, the operators in momentum space, $c^a(\mathbf{k})$, satisfy $c^a(\mathbf{k}) = c^{a\dagger}(-\mathbf{k})$ due to the property $c_i^a = c_i^{a\dagger}$ which leads to standard fermionic anticommutation relation $\{c^{a\dagger}(\mathbf{k}), c^{b\dagger}(\mathbf{k}')\} = \{c^a(\mathbf{k}), c^b(\mathbf{k}')\} = 0$, $\{c^a(\mathbf{k}), c^{b\dagger}(\mathbf{k}')\} = \delta_{ab}\delta(\mathbf{k} - \mathbf{k}')$. We have

$$H^{\mathrm{MMF}}(\mathbf{k}) = \begin{pmatrix} H_{AA}(\mathbf{k}) & H_{AB}(\mathbf{k}) \\ H_{BA}(\mathbf{k}) & H_{BB}(\mathbf{k}) \end{pmatrix},$$

where A, B are the two sublattices in which the original lattice is divided. Since the spin operators are expressed through four Majorana fermions $\{c, b^x, b^y, b^z\}$, each block, H_{ab} with $a, b = A, B$ is a 4×4 matrix.

The Hamiltonian block associated with sites in the same sublattice, $a = A, B$, reads

$$H_{aa}(\mathbf{k}) = \begin{pmatrix} H_{aa}^{00}(\mathbf{k}) & -\frac{i}{4}\lambda_{ax} & -\frac{i}{4}\lambda_{ay} & -\frac{i}{4}\lambda_{az} \\ \frac{i}{4}\lambda_{ax} & H_{aa}^{xx}(\mathbf{k}) & \frac{i}{4}\lambda_{az} & -\frac{i}{4}\lambda_{ay} \\ \frac{i}{4}\lambda_{ay} & -\frac{i}{4}\lambda_{az} & H_{aa}^{yy}(\mathbf{k}) & \frac{i}{4}\lambda_{ax} \\ \frac{i}{4}\lambda_{az} & \frac{i}{4}\lambda_{ay} & -\frac{i}{4}\lambda_{ax} & H_{aa}^{zz}(\mathbf{k}) \end{pmatrix},$$

where

$$\begin{aligned} H_{aa}^{00}(\mathbf{k}) &= -\frac{iJ_2}{4} \sum_{\langle\langle i_a j_a\rangle\rangle} \sum_\alpha \langle i b_{i_a}^\alpha b_{j_a}^\alpha\rangle e^{i\mathbf{k}\cdot\delta_{i_a j_a}} \\ H_{aa}^{\alpha\alpha}(\mathbf{k}) &= -\frac{iJ_2}{4} \sum_{\langle\langle ij\rangle\rangle} \langle i c_{i_a} c_{j_a}\rangle e^{i\mathbf{k}\cdot\delta_{i_a j_a}}, \end{aligned} \tag{A6}$$

with $\alpha = x, y, z$.

The Hamiltonian block associated with the $A - B$ interaction reads

$$H_{AB}(\mathbf{k}) = \begin{pmatrix} H_{AB}^{00}(\mathbf{k}) & 0 & 0 & 0 \\ 0 & H_{AB}^{xx}(\mathbf{k}) & 0 & 0 \\ 0 & 0 & H_{AB}^{yy}(\mathbf{k}) & 0 \\ 0 & 0 & 0 & H_{AB}^{zz}(\mathbf{k}) \end{pmatrix},$$

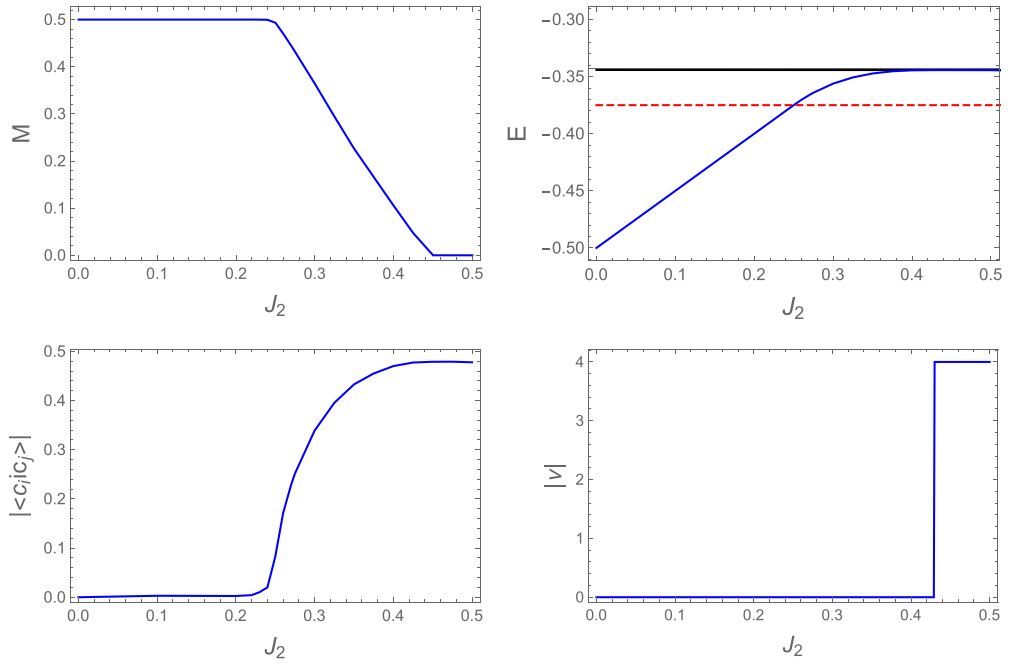

FIG. 7. Dependence of properties of various MMFT solutions with J_2. From top to bottom: AF moment (M), energy per site (E) absolute value of π-QSL amplitude ($|\langle c_i ic_j\rangle|$), and Chern number ($|\nu|$) are shown for the hybrid π-QSL (blue solid lines). The energies of the spin disordered VBC (red solid line) and the pure ($M = 0$) π-QSL (black solid line) are also shown for comparison. $J_1 = 1$ in this plot.

where

$$H^{00}_{AB}(\mathbf{k}) = -\frac{iJ_1}{4}\sum_{\langle i_A j_B\rangle}\sum_{\alpha}\left\langle ib^{\alpha}_{i_A} b^{\alpha}_{j_B}\right\rangle e^{i\mathbf{k}\cdot\delta_{i_A j_B}}$$
$$H^{\alpha\alpha}_{AB}(\mathbf{k}) = -\frac{iJ_1}{4}\sum_{\langle i_A j_B\rangle}\left\langle ic^{\alpha}_{i_A} c^{\alpha}_{j_B}\right\rangle e^{i\mathbf{k}\cdot\delta_{i_A j_B}}. \tag{A7}$$

The self-consistent loop proceeds as follows. A random guess of variational parameters $\langle ic^{\alpha}_{i_a} c^{\alpha}_{j_b}\rangle$, $\langle ib^{\alpha}_{i_a} b^{\alpha}_{j_b}\rangle$ is injected in $H^{MMF}(\mathbf{k})$ and the Hamiltonian diagonalized. The set of Lagrange multipliers $\{\lambda_i\}$ is fixed by the single occupancy constraint in Eq. (A3) using a least-squares minimization. Finally, we find a new set of variational parameters obtained from the mean-field GS which is a Slater determinant constructed from the filled orbitals of the mean-field Hamiltonian. These three steps are repeated until convergence with the desired tolerance is reached.

We now analyze the π-flux solution to the J_1-J_2 Heisenberg model discussing the role played by Néel AF. We also explore other possible quantum spin disordered solutions such as the VBC. We focus on the $0 < J_2 < 0.5$ regime which is sufficient for our purposes.

1. π-QSL solution

For the π-flux QSL bond pattern shown in Fig. 1 of the main text, the Majorana mean-field Hamiltonian is

$$H^{00}_{AA}(\mathbf{k}) = J_2\sum_{\alpha}\left\langle b^{\alpha}_{i_A} ib^{\alpha}_{j_A}\right\rangle\cos(k_x)\sin(k_y)$$
$$H^{\alpha\alpha}_{AA}(\mathbf{k}) = J_2\left\langle c_{i_A} ic_{j_A}\right\rangle\cos(k_x)\sin(k_y),$$
$$H^{00}_{AB}(\mathbf{k}) = i\frac{J_1}{4}\sum_{\alpha}\left\langle b^{\alpha}_{iA} ib^{\alpha}_{jB}\right\rangle(-2i\sin(k_x) + 2\cos(k_y))$$
$$H^{\alpha\alpha}_{AB}(\mathbf{k}) = i\frac{J_1}{4}\langle c_{iA} ic_{jA}\rangle(-2i\sin(k_x) + 2\cos(k_y)), \tag{A8}$$

where $\langle c_{i_A} ic_{j_B}\rangle = \langle b^{\alpha}_{i_A} ib^{\alpha}_{j_B}\rangle > 0$, and $\langle b^{\alpha}_{i_A} ib^{\alpha}_{j_A}\rangle = \langle c_{i_A} ic_{j_A}\rangle < 0$ with $\alpha = x, y, z$ for the flux pattern in Fig. 1 which has a Chern number of $\nu = -4$. Also we have $H^{00}_{BB}(\mathbf{k}) = -H^{00}_{AA}(\mathbf{k})$ and $H^{\alpha\alpha}_{BB}(\mathbf{k}) = -H^{\alpha\alpha}_{AA}(\mathbf{k})$.

The resulting Majorana dispersions can be obtained analytically, $\pm 3\gamma(\mathbf{k})$, $\pm\gamma(\mathbf{k})$ (triply degenerate), with

$$\gamma(\mathbf{k}) = \frac{J_1}{2}\sqrt{c_1^2(\sin^2(k_x) + \cos^2(k_y)) + \left(\frac{J_2}{J_1}\right)^2(2c_2\cos(k_x)\sin(k_y))^2}, \tag{A9}$$

where $c_1 = \langle c_{iA} ic_{jB}\rangle = \langle b^{\alpha}_{i_A} ib^{\alpha}_{j_B}\rangle$, $c_2 = \langle c_{i_A} ic_{j_A}\rangle = \langle b^{\alpha}_{i_A} ib^{\alpha}_{j_A}\rangle$. These are the expressions quoted in the main text.

The dependence of the π-QSL energy with J_2/J_1 is shown in Fig. 7. The energy is almost constant in the range shown: $E(J_2 = 0) = -0.3442$, $E(J_2 = 0.5) = -0.3443$. The lowering of the energy with J_2 due to the opening of the topological gap is evident, for instance, $E(J_2 = 1) = -0.372675$.

2. π-QSL + Néel AF

An important aspect of the physics of undoped cuprates though, which we have ignored up to now, is Néel AF. For $J_2 = 0$ we expect a Néel state in the square lattice. We have searched for hybrid π-flux QSL + Néel AF solutions. Indeed a nonzero AF moment is present for $0 < J_2 < 0.43$ as shown in Fig. 7. For $J_2 < 0.25$ the Néel-AF is fully saturated, $M = 0, 5$, and so the energy follows the classical linear dependence with J_2: $E_{\text{Néel}} = -0.5 + 0.5J_2$ (taking $J_1 = 1$) shown in Fig. 7. In contrast, for $0.24 < J_2 < 0.43$, a π-QSL + Néel AF, i.e., a state having $M < 0.5$ and $|\langle c_i c_j \rangle| \neq 0$ arises. A topological transition occurs at $J_2 \sim 0.43$ where Néel AF fades away and the pure π-QSL with $|\nu| = 4$ wins. Figure 7 indeed shows how the energy of the π-QSL+Néel AF converges to the energy of the pure π-QSL a J_2/J_1 at sufficiently large J_2/J_1.

Although our MMFT π-QSL + Néel AF is always gapped, the gap for $J_2 < 0.43$ associated with the Néel order is trivial while the gap for $J_2 > 0.43$ in the π-QSL phase is topological with Chern number, $|\nu| = 4$. Hence even though a hybrid π-flux QSL + Néel AF actually occurs in the MMFT equations, such state is nontopological; in fact, only the pure π-QSL is topological. However, this could be an artifact of the MMFT in which broken symmetry states are treated classically.

The hybrid π-QSL + Néel AF state is not the lowest energy state in the whole $0 < J_2/J_1 < 0.5$ range. The spin disordered VBC consisting of singlets between n.n. spins has an energy per site of $E_{VBC} = -0.375\, J_1$ for any J_2/J_1 since the singlets are effectively decoupled. As shown in Fig. 7 the VBC state wins for $J_2/J_1 > 0.25$, actually the onset of the hybrid π-QSL + Néel AF state occurs. Although our total energy analysis suggests that a direct transition from a Néel AF to a VBC occurs around $J_2 \sim 0.25 J_1$, it also indicates that a π-QSL + Néel AF is a possible self-consistent solution of the MMFT. Theories beyond the Majorana mean-field treatment including quantum fluctuations may stabilize a coexistent π-QSL + Néel AF state with nontrivial topological properties.

APPENDIX B: DETAILS ON THE TEMPERATURE DEPENDENCE OF THERMAL HALL CONDUCTIVITY

In the main text we have stated that the thermal Hall conductivity can be fitted in a broad temperature range to a exponential form $\kappa_{xy}/T \propto e^{-T/T_0}$. Such exponential forms are observed experimentally in an intermediate temperature range [5]. Here we provide details about these fits. Our theoretical calculations can be nicely fitted to the following expressions: $\kappa_{xy}/T \sim A + Be^{-T/T_0}$ as shown in Fig. 8. For $J_2/J_1 = 1/3$ the fit is $\kappa_{xy}/T \sim -0.02508 - 1.02225e^{-T/0.015}$, for $J_2/J_1 = 0.5$ the fit is $\kappa_{xy}/T \sim -0.0905446 - 1.13263e^{-T/0.029}$, and for $J_2/J_1 = 1$ the fit is $\kappa_{xy}/T \sim -0.0821182 - 1.41715e^{-T/0.08045}$. Using appropriate parameters for the cuprates $J_1 \sim 0.1eV$ would lead to the temperature scales $T_0(J_2/J_1 = 1/3) \sim 18$K, $T_0(J_2/J_1 = 1/2) \sim 35K$, and $T_0(J_2/J_1) \sim 93.4$ K.

We can compare our theoretical MMFT results with the 2D thermal conductivity obtained from experiments. Experimental data of La_2CuO_4 and $Sr_2CuO_2Cl_2$ have been found to have the T dependence $\kappa_{xy}^{expt}/T \sim (-0.0132 - 3.234e^{-T/T_0^{expt}}) \times 10^{-9} \frac{mW}{K^2}$ with $T_0^{expt} \sim 17K$. The theoretical curve with closest T_0 corresponds (taking $J_1 \sim 0.1$ eV) to $J_2/J_1 = 1/3$ ($T_0 \sim 18$ K) and has the dependence $\kappa_{xy}/T \sim (-0.01618 - 1.2073e^{-T/T_0}) \times 10^{-9} \frac{mW}{K^2}$. Since the cuprates are typically in the low J_2/J_1 parameter regime, we conclude that our MMFT predictions for κ_{xy} are consistent with available experimental data.

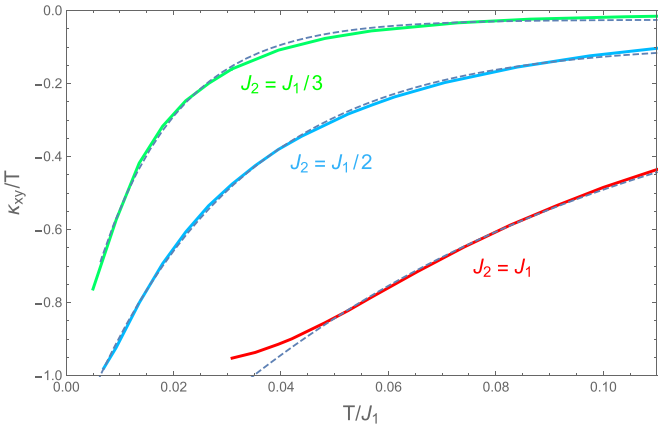

FIG. 8. Exponential temperature dependence of the thermal Hall conductivity. Fits of our calculated MMFT thermal Hall conductivity to $\kappa_{xy}/T \sim A + Be^{-T/T_0}$ are shown.

APPENDIX C: THREE-SPIN MAGNETIC ORBITAL TERM

We now apply the MMFT to the magnetic orbital contribution considered in the main text:

$$H_\phi = J_\phi \sum_{\triangle} \mathbf{S}_i \cdot (\mathbf{S}_j \times \mathbf{S}_k), \tag{C1}$$

where the sum is taken over all triangular plaquettes of the square lattice.

This kind of three-spin term has been discussed in the context of bosonic and fermionic spinon theories of the Hubbard model in the large-U limit [15,17,19]. Actually fermionic mean-field theories provide an exact solution of the large-N limit of the model as has been shown in the SU(N) Heisenberg model [54]. In order to make direct contact with these approaches, we apply the MMFT decoupling directly onto the large-N expression for the chiral three-spin terms. Our starting point is the full expression of the three-spin contribution expressed in terms of Abrikosov fermions [19]:

$$\mathbf{S}_i \cdot (\mathbf{S}_j \times \mathbf{S}_k) = -\frac{i}{4}(P_{ijk} - P_{ijk}^\dagger), \tag{C2}$$

where $P_{ijk} = (f_{i\sigma}^\dagger f_{i\sigma'})(f_{j\sigma'}^\dagger f_{j\sigma''})(f_{k\sigma''}^\dagger f_{k\sigma})$ exchanges three fermions around the triangular plaquette. Note that the Einstein notation for the sums over spin indices is assumed in this section for simplicity. The mean-field treatment of this contribution consists of contracting only the fermionic operators with the same spin, which leads to the large-N expression

$$\mathbf{S}_i \cdot (\mathbf{S}_j \times \mathbf{S}_k) = -\frac{i}{4}[(f_{j\sigma'}^\dagger f_{i\sigma'})(f_{k\sigma''}^\dagger f_{j\sigma''})(f_{i\sigma}^\dagger f_{k\sigma}) - (f_{k\sigma}^\dagger f_{i\sigma})(f_{j\sigma''}^\dagger f_{k\sigma''})(f_{i\sigma'}^\dagger f_{j\sigma'})]. \tag{C3}$$

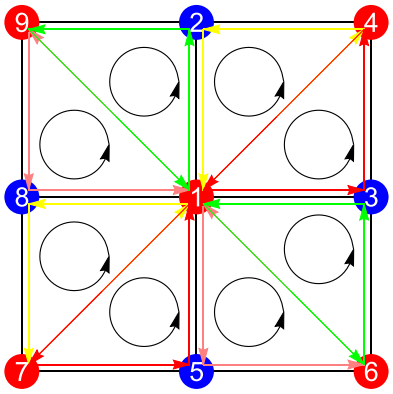

FIG. 9. Three-spin magnetic orbital interactions.

The fermions satisfy $f^\dagger_{i\alpha} f_{i\alpha} = 1$. It can be shown that even for the not so large value $N = 2$ the contractions neglected do not qualitatively change the physics. Defining $\chi_{ij} = f^\dagger_{j\alpha} f_{i\alpha}$ the mean-field Hamiltonian, H_ϕ reads

$$\begin{aligned} H^{MF}_\phi = i\frac{J_\phi}{4}\sum_{\triangle}[&\chi_{ij}\langle\chi_{jk}\rangle\langle\chi_{ki}\rangle - \langle\chi_{ik}\rangle\langle\chi_{kj}\rangle\chi_{ji} \\ &+ \langle\chi_{ij}\rangle\chi_{jk}\langle\chi_{ki}\rangle - \langle\chi_{ik}\rangle\chi_{kj}\langle\chi_{ji}\rangle \\ &+ \langle\chi_{ij}\rangle\langle\chi_{jk}\rangle\chi_{ki} - \chi_{ik}\langle\chi_{kj}\rangle\langle\chi_{ji}\rangle \\ &- 2(\langle\chi_{ij}\rangle\langle\chi_{jk}\rangle\langle\chi_{ki}\rangle - \langle\chi_{ik}\rangle\langle\chi_{kj}\rangle\langle\chi_{ji}\rangle)], \end{aligned} \tag{C4}$$

where the sum is over all triangular plaquettes with vertices ijk.

Performing a Majorana transformation,

$$\begin{aligned} f_{i\uparrow} &= \tfrac{1}{2}\big(c_i - ib^z_i\big), \quad f^\dagger_{i\uparrow} = \tfrac{1}{2}\big(c_i + ib^z_i\big) \\ f_{i\downarrow} &= \tfrac{1}{2}\big(b^y_i - ib^x_i\big), \quad f^\dagger_{i\downarrow} = \tfrac{1}{2}\big(b^y_i + ib^x_i\big), \end{aligned} \tag{C5}$$

leads to the decomposition in terms of the Majoranas

$$\begin{aligned} f^\dagger_{i\alpha} f_{j\alpha} = \tfrac{1}{4}\big(&c_i c_j - ic_i b^z_j + ib^z_i c_j + b^z_i b^z_j + b^y_i b^y_j \\ &- ib^y_i b^x_j + ib^x_i b^y_j + b^x_i b^x_j\big). \end{aligned} \tag{C6}$$

We consider mean-field solutions with nonzero bond fluxes i.e., $\langle\chi_{ij}\rangle = \pm iR_{ij}$ with $R_{ij} \in \mathbb{R}$ leading to the terms

$$\begin{aligned} &\langle\chi_{jk}\rangle\langle\chi_{ki}\rangle f^\dagger_{i\alpha} f_{j\alpha} - \langle\chi_{ik}\rangle\langle\chi_{kj}\rangle f^\dagger_{j\alpha} f_{i\alpha} \\ &\quad = \pm\tfrac{1}{4}R_{jk}R_{ki}\big[(c_i c_j - c_j c_i) + \big(b^x_i b^x_j - b^x_j b^x_i\big) \\ &\qquad + \big(b^y_i b^y_j - b^y_j b^y_i\big) + \big(b^z_i b^z_j - b^z_j b^z_i\big)\big], \end{aligned} \tag{C7}$$

where the final overall sign in front depends on the final bond flux orientation. Hence the final Hamiltonian, H^{MF}_ϕ, will only contain diagonal contributions. Since H^{MF}_ϕ as well as the Heisenberg Hamiltonian is diagonal in the Majoranas, we have that

$$R_{ij} = \frac{1}{4}\left(\langle c_i c_j\rangle + \sum_\alpha \big\langle b^\alpha_i b^\alpha_j\big\rangle\right). \tag{C8}$$

The eight three-spin plaquettes renormalizing the Heisenberg exchange couplings between an A spin and its nearest-neighbor B and also its next-nearest-neighbor B spin are shown in Fig. 9. While the three-spin terms

$$\mathbf{S}_1 \cdot (\mathbf{S}_4 \times \mathbf{S}_2 + \mathbf{S}_3 \times \mathbf{S}_4 + \mathbf{S}_8 \times \mathbf{S}_7 + \mathbf{S}_7 \times \mathbf{S}_5) \tag{C9}$$

are involved in the $1-4$ and $1-7$ n.n.n. couplings, the terms

$$\mathbf{S}_1 \cdot (\mathbf{S}_6 \times \mathbf{S}_3 + \mathbf{S}_5 \times \mathbf{S}_6 + \mathbf{S}_2 \times \mathbf{S}_9 + \mathbf{S}_9 \times \mathbf{S}_8) \tag{C10}$$

renormalize the n.n.n. $1-6$ and $1-9$ exchange couplings. On the other hand, the terms

$$\begin{aligned} \mathbf{S}_1 \cdot (&\mathbf{S}_3 \times \mathbf{S}_2 + \mathbf{S}_3 \times \mathbf{S}_4 + \mathbf{S}_6 \times \mathbf{S}_3 + \mathbf{S}_5 \times \mathbf{S}_3 + \mathbf{S}_2 \times \mathbf{S}_8 \\ &+ \mathbf{S}_9 \times \mathbf{S}_8 + \mathbf{S}_8 \times \mathbf{S}_7 + \mathbf{S}_8 \times \mathbf{S}_5) \end{aligned}$$

renormalize the n.n. $1-3$ and $1-8$ couplings, while

$$\begin{aligned} \mathbf{S}_1 \cdot (&\mathbf{S}_2 \times \mathbf{S}_9 + \mathbf{S}_2 \times \mathbf{S}_8 + \mathbf{S}_4 \times \mathbf{S}_2 + \mathbf{S}_3 \times \mathbf{S}_2 \\ &+ \mathbf{S}_5 \times \mathbf{S}_6 + \mathbf{S}_5 \times \mathbf{S}_3 + \mathbf{S}_7 \times \mathbf{S}_5 + \mathbf{S}_8 \times \mathbf{S}_5), \end{aligned} \tag{C11}$$

the n.n. $1-2$ and $1-5$ couplings.

The three-spin terms evaluated on zero-flux mean-field solutions such as a zero-flux QSL or a VBC solution lead to cancellations so that $\langle H^{MF}_\chi = 0\rangle$. Hence to illustrate the effect of the three-spin terms we evaluate H^{MF}_χ on a π-QSL bond pattern. Introducing the corresponding MMFT bond amplitudes $\langle c_i ic_j\rangle$ and $\langle b^\alpha_i ib^\alpha_j\rangle$ in R_{ij} we find the complete mean-field Hamiltonian (including the Heisenberg contribution)

$$\begin{aligned} H^{00}_{AA}(\mathbf{k}) &= \left(J_2\sum_\alpha \big\langle b^\alpha_{i_A} ib^\alpha_{j_A}\big\rangle + J_\phi R_1^2\right)\cos(k_x)\sin(k_y) \\ H^{\alpha\alpha}_{AA}(\mathbf{k}) &= \big(J_2\big\langle c_{i_A} ic_{j_A}\big\rangle + J_\phi R_1^2\big)\cos(k_x)\sin(k_y), \\ H^{00}_{AB}(\mathbf{k}) &= \frac{i}{4}\left(J_1\sum_\alpha \big\langle b^\alpha_{iA} ib^\alpha_{jB}\big\rangle + J_\phi R_1 R_2\right) \\ &\quad \times(-2i\sin(k_x) + 2\cos(k_y)) \\ H^{\alpha\alpha}_{AB}(\mathbf{k}) &= \frac{i}{4}(J_1\langle c_{iA} ic_{jA}\rangle + J_\phi R_1 R_2)(-2i\sin(k_x) + 2\cos(k_y)), \end{aligned} \tag{C12}$$

where $R_{ij} = R_1$ for nearest-neighbor and $R_{ij} = R_2$ for next-nearest-neighbor bonds. We also have $H^{00}_{BB}(\mathbf{k}) = -H^{00}_{AA}(\mathbf{k})$ and $H^{\alpha\alpha}_{BB}(\mathbf{k}) = -H^{\alpha\alpha}_{AA}(\mathbf{k})$. From the mean-field Hamiltonian derived in Eq. (C12), it is evident that the three-spin terms just modify the bare Heisenberg amplitudes of the π-QSL solution. It is worth noting that even a pure H_ϕ model with infinitesimally small nonzero J_ϕ will induce a π-QSL on the square lattice.

APPENDIX D: DETAILS ON SO COUPLING EFFECTS

For each set of DM vectors defined in the main text, we have systematically compared the energies of the two most relevant ansatze found by the MMFT, namely the VBC state and the π-QSL state. This is displayed in Fig. 10.

Three important features can be noted. First, the π-QSL is always a stable anstaz of our MMFT. Second, the VBC is always lower in energy than the π-QSL, whatever the choice of the DM vectors. Finally, the π-QSL is also always lowered with respect to D indicating that the effect of SO coupling is positive, in the sense that it continues to favor it even though it is an excited state.

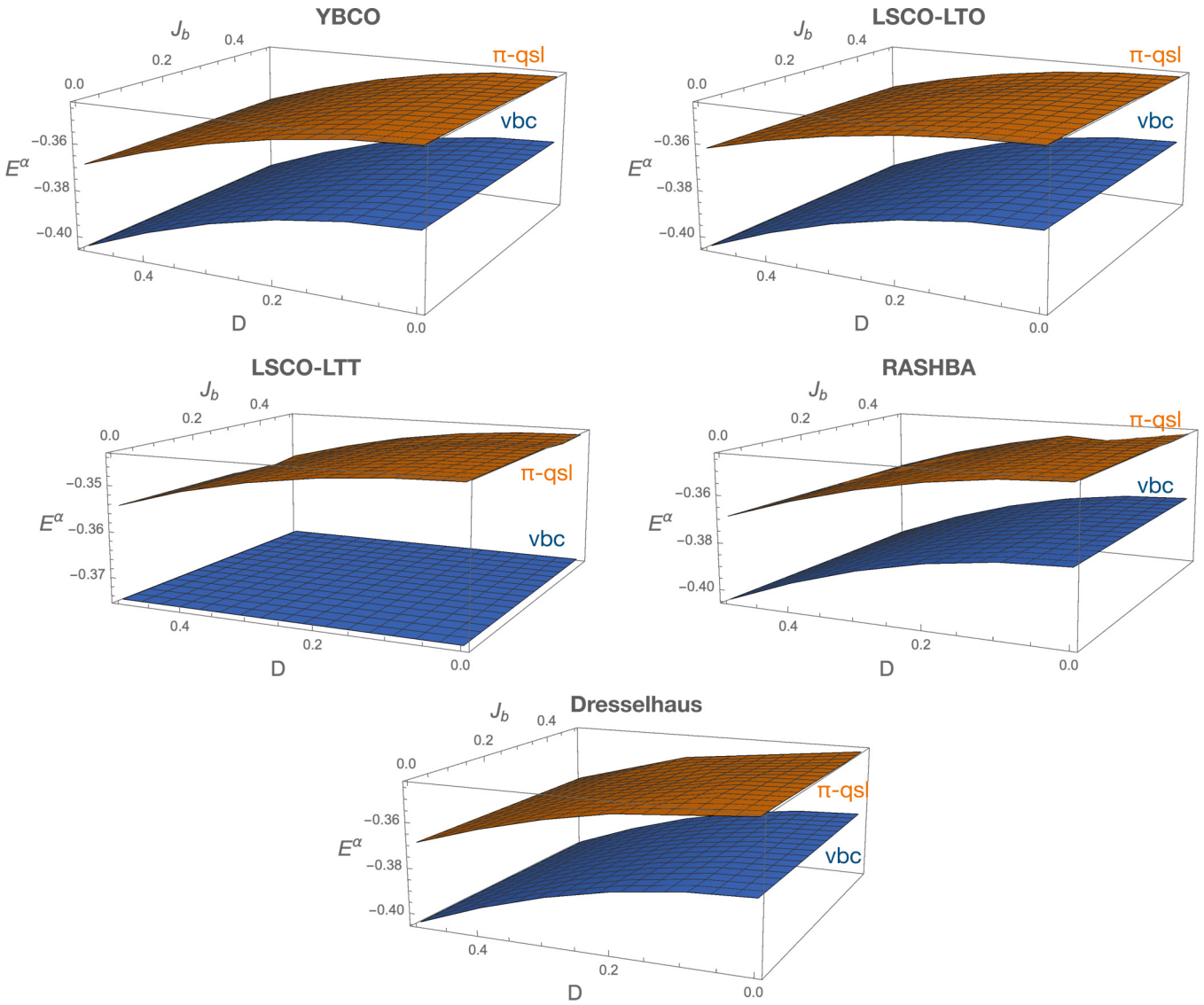

FIG. 10. Comparison of the energy of the VBC and the π-QSL ansatze for the five compatible DM vector choices. The π-QSL always remains an excited state with respect to the VBC one, but the effect of D is to lower its energy hence indicating a positive effect of SO coupling onto this state.

In Fig. 4, we have shown the five distinct domains separated by zero gap lines (white regions). As said, in order to characterize these phases we have calculated the quantum fidelity $|\langle\psi_{\rm ref}|\psi_0\rangle|$ in the whole parameter space by starting from 4 reference states $|\psi_{\rm ref}\rangle$ chosen deep in their corresponding expected parameter regions. They are indicated by black points in Fig. 11 for each of the four panels, and the value of the quantum fidelity, ranging from 0 to 1, scales from white (0) to full colored (1) hexagons respectively. Strikingly, already on such a limited cluster, the fidelity gives strong indications about the phase boundary locations. For instance, from the overlap with the pure Néel state obtained at $J_1 = 1$, we find that the Néel region extends in the lower right part of the ternary plot (yellow points). A very small, yet finite, fidelity can be found in the DM region as J_1 decreases, but considering that the Néel region is unambiguously characterized by a fidelity close to one then, along the $J_2 = 0$ line, the Néel region ends around $J_1 \simeq 0.4$. What is remarkable here is that the Néel, the DM and the collinear regions are well separated even when the transition is second order (no level crossings). As previously mentioned, starting from a different reference state allows us to span entire regions of this model with close-to-one fidelities. This is in particular the case for the intermediate region (blue centered domain of the upper-left panel of Fig. 11) delimited by a frontier of zero energy gap as can be observed in Fig. 5. This region (the blue one in Fig. 11) is gapped and possibly magnetically disordered since the spin structure factor, $S(\mathbf{Q})$, is rather featureless displaying only weak structures as shown in Fig. 12. We have denoted this intermediate phase the DM state in the main text. Finally, at large D, the system enters a fourth phase which is magnetically ordered. This can be interpreted as a quantum version of the magnetic DM state obtained with the MMFT approach. To the best of our knowledge, the intermediate possibly disordered DM state has never been reported so far.

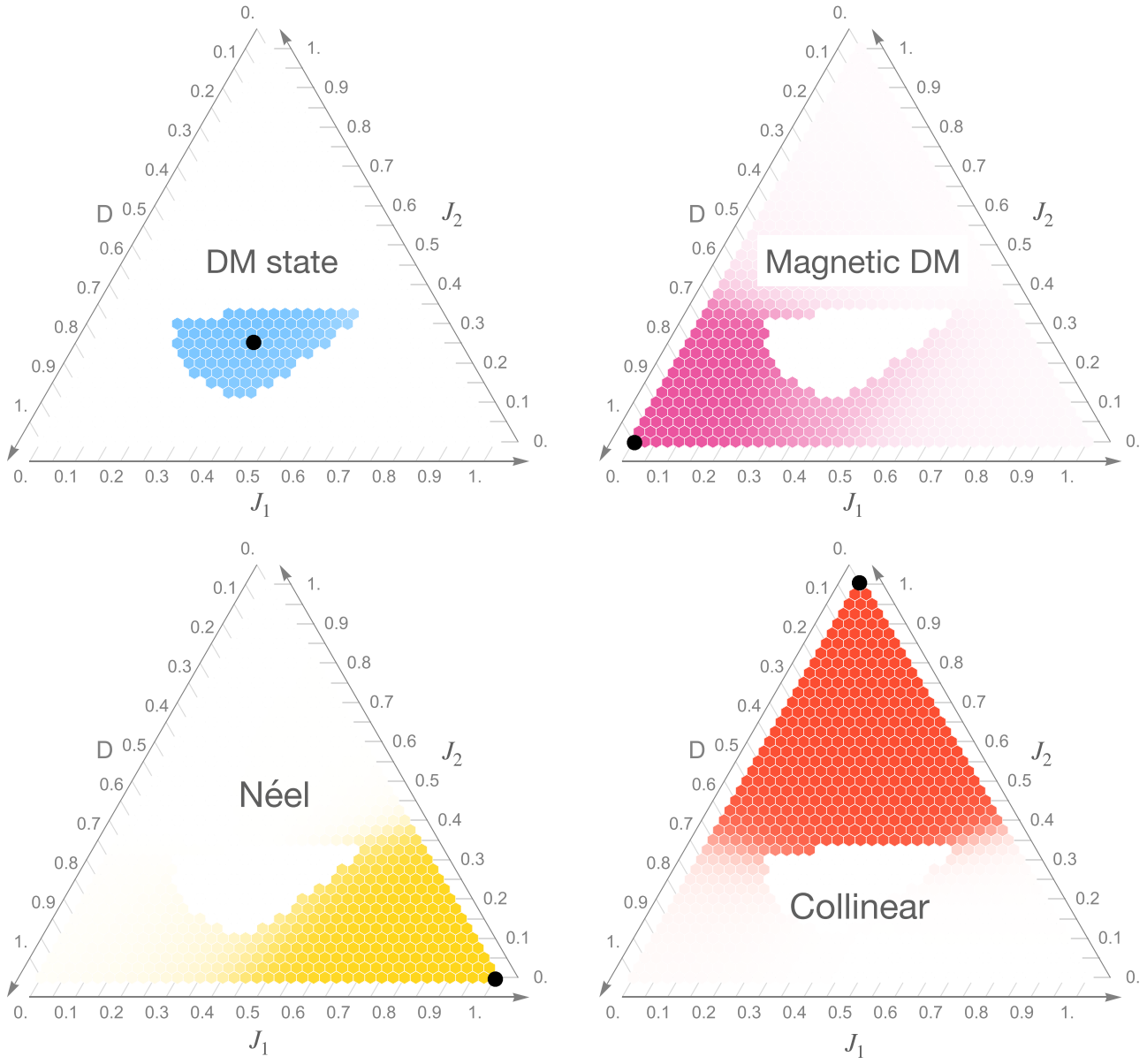

FIG. 11. Quantum fidelity computed by ED for 4 different reference sites (black points). A quantum fidelity of 1 corresponds to full colored point while a zero one corresponds to white hexagons. Four clear regions can be clearly identified, as mentioned in Fig. 5. The disordered phase of the raw $J_1 - J_2$ model cannot be clearly identified in such a small cluster, but clearly appears in the gap of Fig. 5 (extended white region).

APPENDIX E: MAGNETIC ORDER FROM ED

The various magnetic orders in the models considered are investigated by evaluating the ED static spin structure factor:

$$S(\mathbf{Q}) = \frac{1}{N} \sum_{ij} e^{i\mathbf{Q}\cdot(\mathbf{R}_i - \mathbf{R}_j)} \langle \mathbf{S}_i \cdot \mathbf{S}_j \rangle, \tag{E1}$$

where N is the number of sites of the cluster.

In Fig. 12 we compare the $S(\mathbf{Q})$ calculated on a 4×4 cluster for different parameters of the $J_1 - J_2 - D$ and $J_1 - J_2 - J_\phi$ models. The Néel and collinear phases display a large clear structure at their corresponding (π, π) and $(\pi, 0)$ ordering wave vectors, respectively. This behavior is in contrast to the structureless $S(\mathbf{Q})$ of the possible spin disordered phase (around $J_2/J_1 = 0.6$) or the weak structure around $(\pi, 0)$ $((\pi, \pi/2))$ of the J_ϕ (D) dominated phase. The fact that these three last phases display comparable value of $S(\mathbf{Q})$ indicate that they are disordered or very weakly magnetically ordered.

APPENDIX F: MAGNETIC ORBITAL MODEL ED PHASE DIAGRAM

Repeating the same calculation of the quantum fidelity for the J_ϕ model allows for deriving the complete ternary phase diagram with constraint $J_1 + J_2 + J_\phi = 1$. This is displayed in Fig. 13.

At the opposite of the pure DM model, the orbital magnetic effect does not possess first-order transitions to a fourth and intermediate phase, but only continuous transitions between the three limiting cases, Néel (yellow), Collinear (red) and

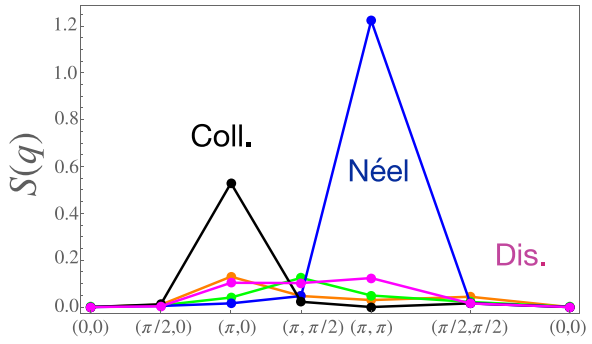

FIG. 12. Effect of J_ϕ and D on magnetic order of the Heisenberg model on the square lattice. The spin structure factor, $S(\mathbf{Q})$, obtained from ED on a 4×4 cluster is shown along the path in the first Brillouin zone of Fig. 1 of the main text. We compare the $S(\mathbf{Q})$ in the Néel, $J_2/J_1 = 0, J_\phi = D = 0$ (blue line) collinear, $J_2/J_1 = 1, J_\phi = D = 0$ (black line), spin disordered, $J_2/J_1 = 0.6, J_\phi = D = 0$ (pink line), $J_2/J_1 = 0.6, J_\phi = 1, D = 0$ (orange line) and D-state $J_2/J_1 = 0.6, D = 1$ (green line). $S(\mathbf{Q})$ is only evaluated at the points shown so the lines are just guides for the eye.

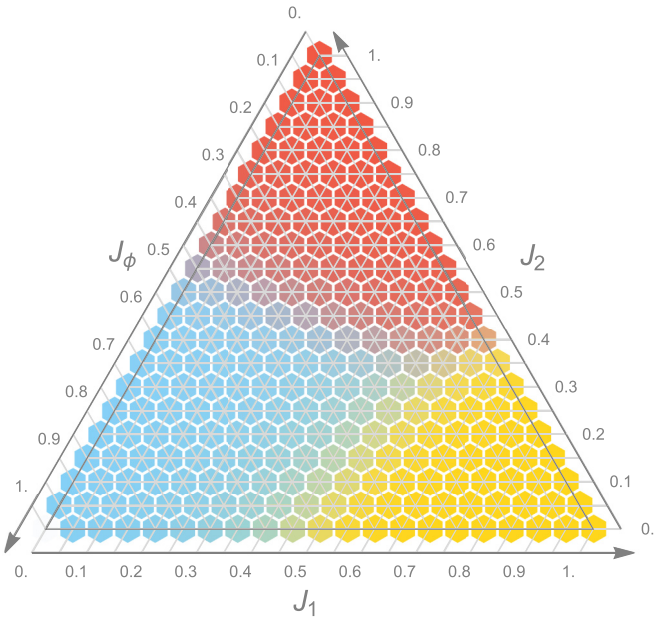

FIG. 13. Ternary phase diagram of the J_ϕ model obtained from quantum fidelities based on three reference points located at the corners (the three colors).

pure disordered state (blue). This shows that, even close in their formal expression, the SO and the orbital magnetic effect behave differently.

[1] G. Grissonnanche *et al.*, Giant thermal Hall conductivity in the pseudogap phase of cuprate superconductors, Nature (London) **571**, 376 (2019).

[2] D. Watanabe *et al.*, Emergence of nontrivial magnetic excitations in a spin-liquid state of Kagomé volborthite, Proc. Natl. Acad. Sci. U.S.A. **113**, 8653 (2016).

[3] Y. Kasahara *et al.*, Unusual Thermal Hall Effect in a Kitaev Spin Liquid Candidate α-$RuCl_3$, Phys. Rev. Lett. **120**, 217205 (2018).

[4] Y. Kasahara *et al.*, Majorana quantization and half-integer thermal quantum Hall effect in a Kitaev spin liquid, Nature (London) **559**, 227 (2018).

[5] G. Grissonnanche *et al.*, Chiral phonons in the pseudogap phase of cuprates, Nat. Phys. **16**, 1108 (2020).

[6] C. M. Varma, Thermal Hall effect in the pseudogap phase of cuprates, Phys. Rev. B **102**, 075113 (2020).

[7] M.-E. Boulanger *et al.*, Thermal Hall conductivity in the cuprate Mott insulators Nd_2CuO_4 and $Sr_2CuO_2Cl_2$, Nat. Commun. **11**, 5325 (2020).

[8] L. Balents, Spin liquids in frustrated magnets, Nature (London) **464**, 199 (2010).

[9] B. J. Powell and R. H. Mckenzie, Quantum frustration in organic Mott insulators: from spin liquids to unconventional superconductors, Rep. Prog. Phys. **74**, 056501 (2011).

[10] A. Pustogow, Thirty-Year Anniversary of κ-$(BEDT\text{-}TTF)_2Cu_2(CN)_3$: Reconciling the Spin Gap in a Spin-Liquid Candidate, Solids **3**, 93 (2022).

[11] C. Lacroix, P. Mendels, and F. Mila (eds.), *Introduction to Frustrated Magnetism: Materials, Experiments, Theory*, Springer Series in Solid-State Sciences (Springer, 2011).

[12] L. Savary and L. Balents, Quantum spin liquids: A review, Rep. Prog. Phys. **80**, 016502 (2017).

[13] Y. Zhou, K. Kanoda, and T. K. Ng, Quantum spin liquid states, Rev. Mod. Phys. **89**, 025003 (2017).

[14] C. Broholm, R. J. Cava, S. A. Kivelson, D. G. Nocera, M. R. Norman, and T. Senthil, Quantum spin liquids, Science **367**, 6475 (2020).

[15] R. Samajdar, S. Chatterjee, S. Sachdev, and M. S. Scheurer, Thermal Hall effect in square-lattice spin liquids: A Schwinger boson mean-field study, Phys. Rev. B **99**, 165126 (2019).

[16] R. Samajdar, M. S. Scheurer, S. Chatterjee, H. Guo, C. Xu, and S. Sachdev, Enhanced thermal Hall effect in the square-lattice Néel state, Nat. Phys. **15**, 1290 (2019).

[17] J. H. Han, J.-H. Park, and P. A. Lee, Consideration of thermal Hall effect in undoped cuprates, Phys. Rev. B **99**, 205157 (2019).

[18] Z.-X. Li and D.-H. Lee, The thermal Hall conductance of two doped symmetry-breaking topological insulators, arXiv:1905.04248.

[19] O. I. Motrunich, Orbital magnetic field effects in spin liquid with spinon Fermi sea: Possible application to κ-$(ET)_2Cu_2(CN)_3$, Phys. Rev. B **73**, 155115 (2006).

[20] I. Dzyaloshinsky, A thermodynamic theory of "weak" ferromagnetism of antiferromagnetics, J. Phys. Chem. Solids **4**, 241 (1958).

[21] T. Moriya, Anisotropic superexchange interaction and weak ferromagnetism, Phys. Rev. **120**, 91 (1960).

[22] T. Moriya, New Mechanism of Anisotropic Superexchange Interaction, Phys. Rev. Lett. **4**, 228 (1960).

[23] M. Kawano, Y. Onose, and C. Hotta, Designing Rashba-Drusselhaus effect in magnetic insulators, Commun. Phys. **2**, 27 (2019).

[24] A. Kitaev, Anyons in an exactly solvable model and beyond, Ann. Phys. **321**, 2 (2006).

[25] A. Ralko and J. Merino, Novel Chiral Quantum Spin Liquids in Kitaev Magnets, Phys. Rev. Lett. **124**, 217203 (2020).
[26] Y.-F. Yang, G.-M. Zhang, Universal Behavior of the Thermal Hall Conductivity, Phys. Rev. Lett. **124**, 186602 (2020).
[27] E. H. Lieb, Flux Phase of the Half-Filled Band, Phys. Rev. Lett. **73**, 2158 (1994).
[28] All the phases reported here are well described by a 2-site unit-cell. Note however that at large J_2, the collinear phase can only be obtained on a 4-site unit-cell. For intermediate J_2/J_1 and $D \neq 0$, we also find a mean-field solution made of *plaquettes*. This state is rejected since it decouples all n.n.n. processes and behaves like a classical mean-field GS not compatible with known results neither our ED calculations.
[29] T. Qin, Q. Niu, and J. Shi, Energy Magnetization and the Thermal Hall Effect, Phys. Rev. Lett. **107**, 236601 (2011).
[30] L. Wang and A. W. Sandvik, Critical Level Crossings and Gapless Spin Liquid in the Square-Lattice Spin-1/2 $J_1 - J_2$ Heisenberg Antiferromagnet, Phys. Rev. Lett. **121**, 107202 (2018).
[31] F. Ferrari and F. Becca, Gapless spin liquid and valence-bond solid in the $J_1 - J_2$ Heisenberg model on the square lattice: Insights from singlet and triplet excitations, Phys. Rev. B **102**, 014417 (2020).
[32] W.-Y. Liu, S.-S. Gong, Y.-B. Li, D. Poilblanc, W.-Q. Chen, Z.-C. Gu, Gapless quantum spin liquid and global phase diagram of the spin-1/2 $J_1 - J_2$ square antiferromagnetic Heisenberg model, arXiv:2009.01821.
[33] Y. Nomura and M. Imada, Dirac-Type Nodal Spin Liquid Revealed by Refined Quantum Many-Body Solver Using Neural-Network Wave Function, Correlation Ratio, and Level Spectroscopy, Phys. Rev. X **11**, 031034 (2021).
[34] R. R. P. Singh, Z. Weihong, C. J. Hamer, and J. Oitmaa, Dimer order with striped correlations in the $J_1 - J_2$ Heisenberg model Phys. Rev. B **60**, 7278 (1999).
[35] H.-C. Jiang, H. Yao, and L. Balents, Spin liquid ground state of the spin-1/2 square $J_1 - J_2$ Heisenberg model, Phys. Rev. B **86**, 024424 (2012).
[36] V. Kalmeyer and R. B. Laughlin, Equivalence of the Resonating- Valence-Bond and Fractional Quantum Hall States, Phys. Rev. Lett. **59**, 2095 (1987).
[37] A. E. B. Nielsen, G. Sierra, and J. I. Cirac, Local models of quantum Hall states in lattices and physical implications, Nat. Commun. **4**, 2864 (2013).
[38] D. Poilblanc, Investigation of the chiral antiferromagnetic Heisenberg model using projected entangled pair states, Phys. Rev. B **96**, 121118(R) (2017).
[39] M. Kawano and C. Hotta, Thermal Hall effect and topological edge states in a square-lattice antiferromagnet, Phys. Rev. B **99**, 054422 (2019).
[40] D. F. Schroeter, E. Kapit, R. Thomale, and M. Greiter, Spin Hamiltonian for which the Chiral Spin Liquid is the Exact Ground State, Phys. Rev. Lett. **99**, 097202 (2007).
[41] A. E. B. Nielsen, J. I. Cirac, and G. Sierra, Laughlin Spin-Liquid States on Lattices Obtained from Conformal Field Theory, Phys. Rev. Lett. **108**, 257206 (2012).
[42] A. Wietek and A. M. Läuchli, Chiral spin liquid and quantum criticality in extended $S = 1/2$ Heisenberg models on the triangular lattice, Phys. Rev. B **95**, 035141 (2017).
[43] M. Greiter and R. Thomale, Non-Abelian Statistics in a Quantum Antiferromagnet, Phys. Rev. Lett. **102**, 207203 (2009).
[44] M. Greiter, D. F. Schroeter, and R. Thomale, Parent Hamiltonian for the non-Abelian chiral spin liquid, Phys. Rev. B **89**, 165125 (2014).
[45] T. Cookmeyer, J. Motruk, and J. E. Moore, Four-Spin Terms and the Origin of the Chiral Spin Liquid in Mott Insulators on the Triangular Lattice, Phys. Rev. Lett. **127**, 087201 (2021).
[46] B. Bauer, L. Cincio, B. P. Keller, M. Dolfi, G. Vidal, S. Trebst, and A. W. W. Ludwig, Chiral spin liquid and emergent anyons in a Kagomé lattice Mott insulator, Nat. Commun. **5**, 5137 (2014).
[47] L. Messio, B. Bernu, and C. Lhuillier, Kagomé Antiferromagnet: A Chiral Topological Spin Liquid? Phys. Rev. Lett. **108**, 207204 (2012).
[48] S.-S. Gong, W. Zhu, and D. Sheng, Emergent chiral spin liquid: Fractional quantum Hall effect in a Kagomé Heisenberg model, Sci. Rep. **4**, 6317 (2014).
[49] Y.-C. He, D. N. Sheng, and Y. Chen, Chiral Spin Liquid in a Frustrated Anisotropic Kagomé Heisenberg Model, Phys. Rev. Lett. **112**, 137202 (2014).
[50] E. Pavarini, I. Dasgupta, T. Saha-Dasgupta, O. Jepsen, and O. K. Andersen, Band-Structure Trend in Hole-Doped Cuprates and Correlation with $T_{c\,\max}$, Phys. Rev. Lett. **87**, 047003 (2001).
[51] B. Dalla Piazza, M. Mourigal, N. B. Christensen, G. J. Nilsen, P. Tregenna-Piggott, T. G. Perring, M. Enderle, D. F. McMorrow, D. A. Ivanov, and H. M. Roennow, Fractional excitations in the square-lattice quantum antiferromagnet, Nat. Phys. **11**, 62 (2015).
[52] M. Takahashi, Half-filled Hubbard model at low temperature, J. Phys. C: Solid State Phys. **10**, 1289 (1977).
[53] W. Choi, P. W. Klein, A. Rosch, and Y. B. Kim, Topological superconductivity in the Kondo-Kitaev model, Phys. Rev. B **98**, 155123 (2018).
[54] A. Auerbach, *Interacting Electrons and Quantum Magnetism* (Springer, New York, NY, 1994).